Magnetic ripple domain structure in FeGa/MgO thin films

Adrián Begué[a,b], Maria Grazia Proietti[a,b], José I. Arnaudas[a,b,c], Miguel Ciria[a,b]

[a]*Instituto de Ciencia de Materiales de Aragón, Consejo Superior de Investigaciones Científicas, Zaragoza, Spain.*
[b]*Departamento de Física de la Materia Condensada, Universidad de Zaragoza, Zaragoza, Spain.*
[c]*Instituto de Nanociencia de Aragón, Universidad de Zaragoza, Zaragoza, Spain.*

Abstract

The magnetic domain structure is studied in epitaxial $Fe_{100-x}Ga_x$/MgO(001) films with $0 < x < 30$ and thicknesses below 60 nm by magnetic force microscopy. For low gallium content, domains with the magnetization lying in the film plane and domain walls separating micrometric areas are observed. Above $x \approx 20$, the magnetic contrast shows a fine corrugation, ranging from 300 to 900 nm, suggesting a ripple substructure with a periodic oscillation of the magnetization. We discuss the presence of a random magnetic anisotropy contribution, that superimposed to the cubic coherent anisotropy, is able to break the uniform orientation of the magnetization. The origin of that random anisotropy is attributed to several factors: coexistence of crystal phases in the films, inhomogeneous distribution of both internal strain and Ga-Ga next nearest neighbor pairs and interface magnetic anisotropy due to the Fe-O bond.

Keywords:

Epitaxial FeGa films; Magnetic force microscopy; Magnetic anisotropy; Random magnetic anisotropy

---

*Corresponding author
Email address:* `miguel.ciria@csic.es` (Miguel Ciria)

1. Introduction

The Fe-Ga alloys have become an important material for magnetostrictive applications because of their large tetragonal magnetostriction λ_{100} at low field [1, 2, 3] enhanced by the presence of rare earth impurities [4]. The sample microstructure depends on the preparation method and it is customary to obtain samples with ordered $D0_3$ *bcc* crystallites in a disordered A2 *bcc* matrix instead of a mixture of A2 and ordered Ll_2 *fcc* crystal phases [5]. The magnetic properties look to be controlled by the presence of next-nearest neighbors (NNN) Ga-Ga pairs along the cubic [100] directions and its relation with the magnetostrictive property is suggested by the presence of $D0_3$-like inclusions with tetragonal distortion [4]. The Ga pairing along the [100] direction has been also linked to the decrement of the cubic magnetocrystalline four-fold anisotropy constant in this compound [6]. The magnetic behavior is enriched in thin film systems, and a perpendicular magnetic anisotropy (PMA) in epitaxial films is ascribed to a minute asymmetric distribution of these NNN Ga-Ga pairs between in-plane and out-of-plane directions[7]. In FeGa films with thickness above 65 nm, the residual strain can introduce the well-known stripe phase structure [8] due to the presence of weak magnetoelastic (ME) perpendicular anisotropy contribution to the anisotropy energy.

The $Fe_{100-x}Ga_x$/MgO system can combine strong ME coupling of the FeGa alloy into the rich oxide-3d metal interface physics [9]. The overlap between *O-p* and *Fe-d* orbitals induces large values for the interface anisotropy constant K_s [10]. The ME anisotropy contribution could be used to manipulate the magnetic anisotropy in a film grown onto a ferroelectric layer [11], in addition to the modification due to the application of electric field [12].

The study of the magnetic domain configuration in thin films is a tool to insight about the presence of competing interactions with the shape anisotropy. Thus the ME energy due to the coupling between magnetic moment and strain or the interface contribution to the total magnetic anisotropy are responsible for the observation of periodic domain structures [13, 14]. In polycrystalline films,

2

the magnetization can be inhomogeneous, generating the effect known as magnetization ripple [15]. The explanation for the fluctuation of $\mathbf{M}$ is based on the irregular magnetocrystalline anisotropy of the randomly distributed crystallites. The model description incorporates the statistical treatment of local randomly oriented anisotropy and a uniform magnetic anisotropy [16].

Here we present a study of the magnetic domain structure of $Fe_{100-x}Ga_x$ films grown on MgO(001) as function of x performed by magnetic force microscopy (MFM). We show that the presence of a domain structure in $Fe_{100-x}Ga_x$ films evolves from an in-plane disposition of the magnetization to a corrugated domain structure, with periodicities in the range of hundreds of nanometers, as the Ga content increases. Because of the weakness of both volume and interface perpendicular anisotropies, the role of the disorder introduced by the formation of secondary phases as the Ga content increases is discussed. Therefore, the presence of a corrugation of the domain images is related to the presence of a weak random magnetic anisotropy superimposed to the coherent cubic regular contribution.

2. Experimental results

2.1. Thin film preparation

The samples studied here have been grown by Molecular Beam Epitaxy in a process described elsewhere [17], with the substrate temperature T_s set at 150 ^{o}C. The films are grown directly on the MgO(001) surface after as-received substrates are heated at 800 ^{o}C for four hours, in UHV conditions. Reflection high energy electron diffraction pictures show Kikuchi patterns indicating the cleanness of the surface and reveals, in combination with Transmission Electron Microscopy images, the growth of the FeGa(001) films with in-plane axes rotated 45 degrees with respect to the equivalent MgO(001) directions: MgO[110]$\|$$\|$ FeGa[100]. The film thickness t_f ranges between 16 nm to 56 nm and all of them were capped with 2 nm of Mo.

3

x	t_f	$K_{(100)}$	$\Delta K_{(100)}$	$K_{(200)}$	$\Delta K_{(200)}$	L	ϵ
(% Ga)	(nm)	(nm^{-1})	(nm^{-1})	(nm^{-1})	(nm^{-1})	(nm)	
13	17	-	-	6.967	0.156	-	-
21	16	3.438	0.143	6.925	0.185	7.1	0.010
24	20	3.468	0.107	6.930	0.172	12.1	0.011
28	21	3.451	0.081	6.912	0.132	16.6	0.009
28	56	3.406	0.099	6.848	0.146	11.7	0.010

Table 1: Composition and thickness used to identify the samples grown at $T_s = 150$ ^oC presented in this study. Reciprocal space position and Full Width at Half Height (ΔK) for (001) and (002) reflections obtained with Gaussian curve fit. K is defined as $2sin\theta/\lambda$ and ΔK is $cos\theta\Delta(2\theta)/\lambda$. L and ϵ values obtained by performing the fit of the (001) and (002) reflections with the Williamson-Hall model described in the text. The errors for Ga composition is around $\pm$ 1 %, for t_f $\pm$ 0.5 nm, for $K_{(100)} \sim 8 \times10^{-3}nm^{-1}$, for $K_{(200)} \sim 4 \times10^{-4}nm^{-1}$, for $\Delta K_{(100)} \sim 0.03$ nm^{-1} and for $\Delta K_{(200)} \sim 0.001$ nm^{-1}.

Magnetic properties were investigated by vibrating sample magnetometry (VSM), magneto-optic Kerr effect (MOKE) and magnetic force microscopy (MFM) in air and low vacuum. A Rigaku rotating anode D/max 2500 diffractometer working with a Bragg-Brentano configuration with the $K_{\alpha,Cu}$ wavelength was used to perform *ex situ* structural characterization. For the film with x= 28 and t_f= 56 nm, the beamline BM25A at the European Synchrotron Radiation Facility (ESRF), Grenoble, France with $\lambda = 0.062$ nn was used. Dispersive X-ray spectroscopy (EDX) and X-ray reflectivity were used to determine composition and film thickness. Table 1 presents the relevant structural data of the films used in this study. The samples are referred in the text with two of numbers describing composition and thickness, thus 13-17 stands for the film with Ga content 13 % and $t_f = 17$ nm.

2.2. Magnetic force microscopy images

Figure 1 shows atomic force microscopy images on films grown at $T_s = 150$ ^oC and $T_s = 600$ ^oC with *bcc* crystal structure [17]. The image of the films grown
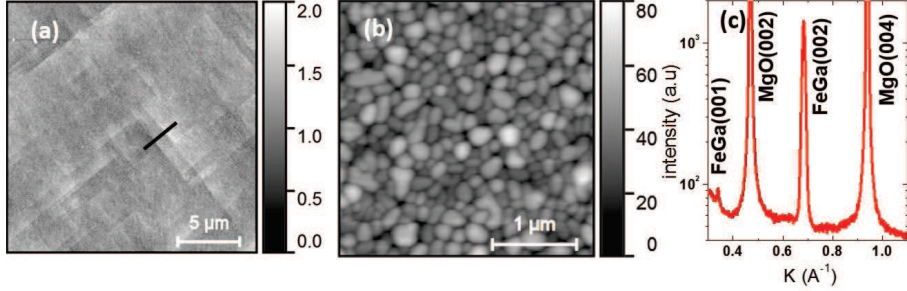
Figure 1: Topographic images taken on films grown at (a) $T_s = 150\ ^o$ C (sample 24-20) and (b) $T_s = 600\ ^o$C. The color bar key units are nm. The height of the steps along the thick line in panel a are about 0.4 nn. (c) X-ray diffraction data, with K($=2sin\theta/\lambda$) perpendicular to the film plane, for sample 28-56.

at $T_s = 150\ ^o$C, obtained from sample 24-20, is representative of the topography

of the films studied by MFM. By elevating T_s, the roughness increases and the film surface looks like a set of domes, notice that the gray scale is larger and the window length side smaller for the films with $T_s = 600\ ^o$C than for the films with $T_s = 150\ ^o$C. Similar transition from 2- to 3- dimensional growing has been reported for pure Fe films grown on MgO [18]. The image taken for the films

grown at 150 ^{o}C shows also some steps due to the MgO [110] edges, the height of which is about 0.4 nm (measured for the steps crossing the black line in Fig 1a). Since samples prepared at 150 ^{o}C did not show 3D growth but two-dimensional, we performed our magnetic analyses only on that kind of samples and not on others prepared at higher temperatures with large roughness that can affect the

magnetic domain structure.

Magnetic force microscopy images presented in Fig 2 were performed in air (a)-(d) and in low vacuum (e)-(f) for the films listed in table 1. For film 13-17 the lines seen in Fig. 2a are interpreted as magnetic domain walls (some tip-induce feature are also observed). These lines separate areas without contrast,

indicating that $\mathbf{M}$ is confined in the plane. Increasing the gallium content, see film 24-20 displayed in Fig 2b, shows a fine structure not observed for film 13-17. Fig 2c and 2d shows the same kind of magnetic contrast, revealing a non

uniform magnetic configuration, in more detail for films with 28-56 and 28-21, respectively. For sample 21-16 strength of the corrugation is very weak for in-air measurements (not shown). These features do not change after performing several scans on the same area of the sample.

Performing MFM measurements in vacuum increases the sensitivity of the technique to measure stray field because of the increment of the cantilever quality factor. Thus, the in-vacuum image for film 13-17 displays only the contrast due to the domain walls (see Fig 2e) without the trace of any other sub-structure, while for sample 21-16 the corrugation becomes very clear (see Fig 2f). A rough comparison of the strength of the contrast for both kind of domain structures is performed considering the range of the variation of the signal for films 13-17 and 21-16 (see Figs 2e and f), because these measurements were obtained in similar in-vacuum conditions. The magnetic signal of sample 21-16 is in the range of ± 1.5 degrees, small compared with that due to the domain walls of film 13-17, which is ± 7 degrees. The inset of Fig 2f represents an image of the film 21-16 in the range of ± 7 degrees. For the films with $x > 21$ the corrugation is clearly observed in the air images (Figs 2b to 2d), although the sensitivity is smaller for this measurements (see that the larger scale is now limited to ± 0.5 degrees). The period of these ripple structures is about 300 nm for samples 24-20, 28-56 and 28-21 and 900 nm for film 21-16.

The lines in image Fig 2a and e can be interpreted as domain walls separating areas with in-plane magnetization and are the expected result for thin films without significant out-of-plane contributions. The texture of the images changes for the films with $x > 20$, for which areas with alternating contrast are observed, see fig 2c-d. This domain structure is obtained in remnant state achieved after applying field along the in-plane direction.

Some MFM images obtained in bulk samples showing similar structures to that shown for samples with $x > 20$, and they were explained by a sample preparation process that can induce stresses and other defects on the sample surface[19]. However, the thin films presented here have not been treated after growth and the observed features cannot been attributed to any post-growing

6

processing. In bulk samples, quenched in water or slowly cooled single-crystals, large domains have been observed without fine magnetic structures [20, 19, 21], resembling the domains obtained for films with low Ga contents seen in Figure 2a, because the magnetic contrast is only due to the presence of domain walls.

It is found that the corrugation of the magnetic contrast in thin films is an indication of the presence of a magnetic anisotropy that competes with the magnetostatic term. Thus, volume perpendicular magnetic anisotropy (Ni [13] and FeGa[8] films), interface magnetic anisotropy (in Co/Pt multilayers with canted magnetization [14]) and random magnetic anisotropy in polycrystalline NiFe films [15] generate the stripe and ripple domain configurations. These contributions will be discussed in the next sections.

2.3. Magnetization loops

A consequence of non-homogeneous domain structure concerns the magnetization curves: if $\mathbf{M}$ has some degree of out-of-plane component or non-collinear distribution, the remanent magnetization M_r has to be lower than the saturation value M_s [13, 8, 14]. Figure 3(a) shows M vs μ_0H for a maximum applied field of 9 T along the in-plane easy direction. This measurement allows subtracting linear diamagnetic contributions with the slope obtained at large field ($\mu_0 H > 6$ T). A correction performed in loops that reach lower values of the maximum field can yield a M_r equal to M_s, see the loop performed up to 0.15 T in Figure 3(a)inset. For the loop taken for sample 28-56, it can be noted that M_r is large, around $0.95 M_s$ but a field of about 1.6 T is needed to reach the full saturation.

Fig 3 shows hysteresis loops performed for samples 13-17, 21-16, 24-20 and 28-56, with the applied field along the FeGa <100> and <110> in-plane directions. For the 13-17 sample the curve with B along the <100> direction presents larger remanence than that performed along the <110> one. The other films present the opposite behavior and the remanence is larger for loops with B along the <110> axis. In bulk crystals [22] and other epitaxial thin films under tensile [7] or compressive [23] stress the easy magnetization direction also moves from
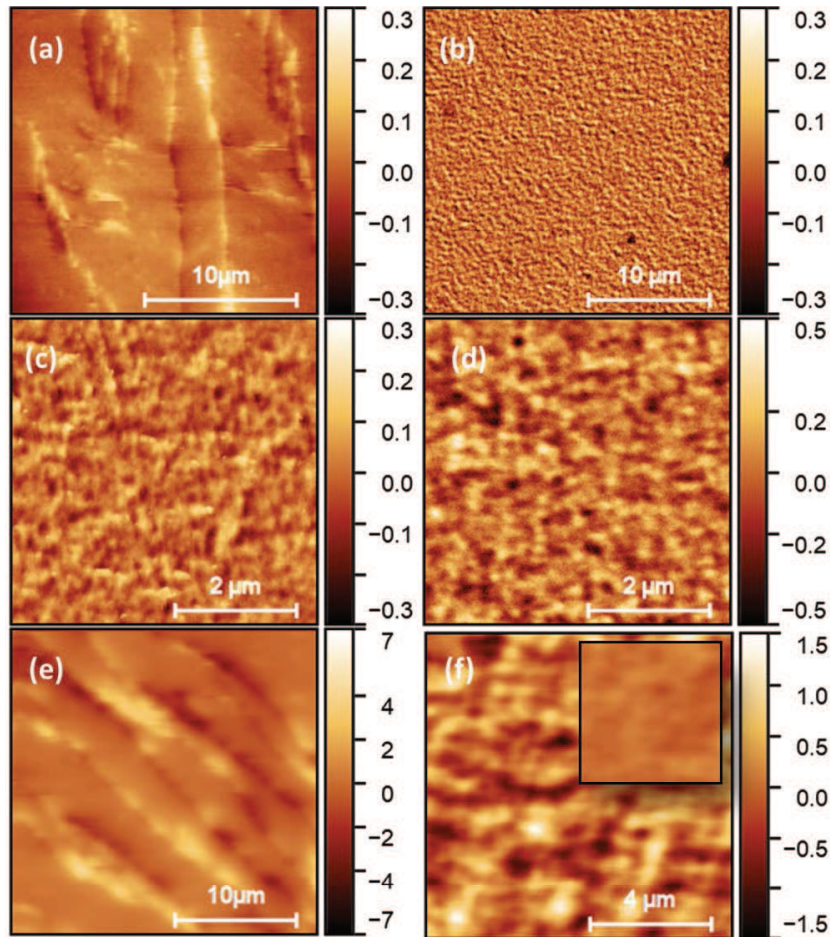
7

Figure 2: Magnetic force microscopy images taken in air for films (a) 13-17 (b) 24-20 (c) 28-56 nm (d) 28-21, and in low-vacuum for films (e) 13-17 and (f) 21-16, the color scale for the inset is ± 7 degrees.
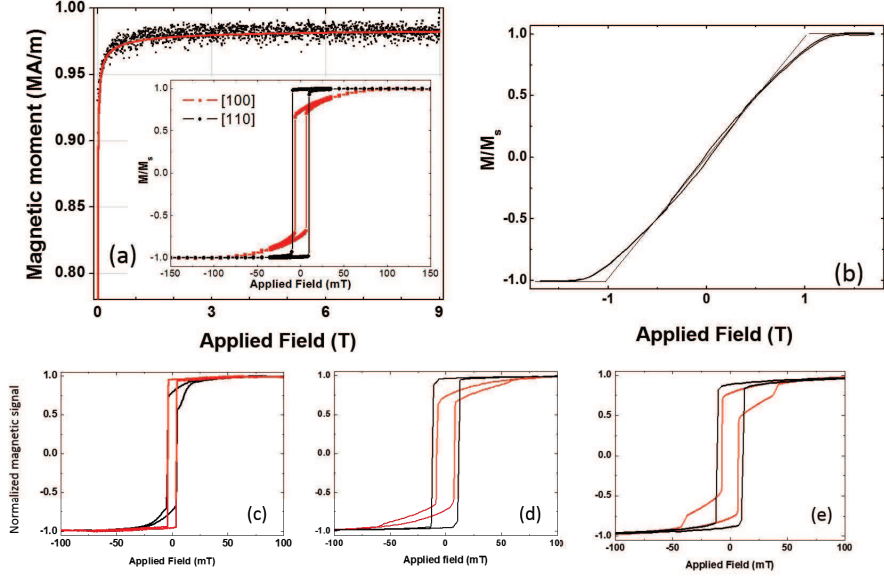
Figure 3: (a) Detail of the magnetization loop with applied field up to 9 T along the easy direction for sample 28-56, red line is a fit described in the text. Inset. MB loops in the low fiend range ($\pm$ 150 mT) for [110] and [100] in-plane directions. (b) M-H loop along the axial [001] direction for sample 28-21. The line is a fit used to calculate the slope at zero field and evaluate the effective magnetic anisotropy constant. In-plane loops for samples (c) 13-17 (d) 21-16 and (e) 24-20. As in the inset of panel a, red and black lines indicate, respectively, magnetic field applied along [100] and [110] directions.

$<100>$ to $<110>$ as the Ga content increases. For the (001) plane the magneto-crystalline energy density $e_{mc}(\phi)$ can be expressed as $K_1 sin^2\phi cos^2\phi$, with K_1 the magnetic anisotropy constant and ϕ the angle that forms $\mathbf{M}$ and the [100] direction. K_1 can be estimated evaluating the energy required to saturate the film along each direction. The measurement for films with x = 28 gives rise to a value of about -10 kJ/m^3 for K_1.

The need of large magnetic field to reach a full saturation cannot be explained by mis-orientation between sample and magnetic field since the magnitude of the anisotropy constant is small, around 10 kJ/m^3. Therefore, the lack of magnetization at low field can be associated with the presence of the domain structure observed in MFM images.

9

2.4. X-ray diffraction

The films presented here have been studied previously by X-ray diffraction [17]. For film 28-56, a scan has been done by means of synchrotron radiation light with $\lambda = 0.062$ nn, see Figure 1c and $K(=2sin\theta/\lambda)$, perpendicular to the film plane. The out-of-plane and in-plane lattice parameter value decreases and

170 increases, respectively, with respect to the bulk value because of the effect of the epitaxial strain due to the MgO substrate [17]. Regarding the ordering of the Ga and Fe atoms, a superlattice (001) peak is observed for x above 20, together with the (002) peak due to the *bcc* structure. The width $\Delta K_{(00n)}$ of those peaks, fitted using gaussian functions, is presented in Table 1.

175 For the measurements obtained with K_α radiation, the effect on the FeGa peak width due to the presence of $K_{\alpha,1}$ and $K_{\alpha,2}$ components can be quantified by considering the splitting of the MgO substrate (002) and (004) reflections, which increases with K. Thus, the correction to the width values of the FeGa peaks can be estimated resulting in negligible changes of $\Delta K_{(001)}$ and $\Delta K_{(002)}$.

180 The fact that $\Delta K_{(002)}$ is larger than $\Delta K_{(001)}$, see values included in Table 1 is explained by the presence of inhomogeneous strain [24]. Sources for this contribution are dislocations, non-uniform distortions, or antiphase domain boundaries [24]. This strain is superimposed to that obtained by the evaluation of the lattice parameters by means of the measurement of the Bragg reflections.

185 The Williamson-Hall method applied to gaussian fits [24, 25] relates $\Delta K_{(00n)}$ to the average crystallite size L and strain ϵ in the film by the equation $\Delta K^2_{(n00)} = (0.9/L)^2 + 4\epsilon^2 K^2$. The values obtained for L and ϵ are presented in table 1. Notice that the value obtained for L is not limited by the film thickness and ϵ values are in the range of 10^{-2} for the samples studied, indicating that the strain

190 in the films is inhomogeneous. The misfit can introduce misfit dislocations that increment ϵ, however the misfit between $Fe_{100-x}Ga_x$ and MgO decreases with x since the bulk lattice parameter of the $Fe_{100-x}Ga_x$ alloy increases with Ga content and gets closer to $\sqrt{2}a_{MgO} \approx 2.977$ Å, a fact that discards the nucleation of misfit dislocations as the origin for an increment of the value of ϵ, and

195 suggests effects that appear with the increment of Ga content. The onset of the

(001) reflection, suggest that the film is formed by crystal regions with ordered and random distribution of Ga/Fe species, corresponding to phases (A2 and D0$_3$) with slightly different lattice parameters [26] that contribute to enlarge the inhomogenous strain in the film as x increases.

3. Analysis

Here, we analyze several contribution to the magnetic energy that can play a role in order to explain the observed inhomogeneous domain structures.

3.1. Perpendicular magnetic anisotropies

The microscopic modulation on the magnetization vector has been ascribed to the competition between perpendicular and shape anisotropies. Several models predict the range of thicknesses that hold a configuration for $\mathbf{M}$ with an out-of-plane component, in terms of the ratio of the perpendicular to shape anisotropy constatns.

3.1.1. Volume anisotropies

The standard model establishes the presence of stripe phase in terms of the parameter $K_u/(0.5\mu_0 M_s^2) = Q$ with K_u being the perpendicular magnetic anisotropy constant. For $Q < 1$, the film thickness has to be larger than the critical value to develop a stripe structure [27]. Figure 3b shows a representative M-H loop, with H perpendicular to the film, for sample 28-21. The thin line corresponds to the linear fit of $M(H)$ used to evaluate the perpendicular anisotropy constant through the anisotropy field H_a, and provides $\mu_0 H_a \approx 1$ T for the intersection with M $= M_s$. In the case of a sole magnetostatic contribution to K_u, $\mu_0 H_a = \mu_0 M_a$. However, several values for $\mu_0 M_s$ are reported in the literature for compositions around $x = 28$, ranging from ≈ 1.4 T [28] to around 1.15 T [26, 29]. Our VSM measurements provide for the film 28-56 a value for $\mu_0 M_s$ of about 1.2 T ($M_s = 0.98$ MA/m), see Fig 3.

For the films presented, the magetostrictive contribution does not induce perpendicular anisotropy because the signs of the film strains[17] and the B_1

11

ME coefficient results in a contribution that favors the in-plane orientation of **M**. The contribution due to an asymmetric distribution of the NNN Ga-Ga pairs proposed to explain the anisotropies in other Fe-Ga films could also explain the presence of a positive K_u [8]. The simplest estimation of K_u can be done by assuming that the total in-plane anisotropies correspond to $0.5\mu_0 M_s^2$. Considering $\mu_0 M_s =1.2$ T and the value of $\mu_0 H_a \approx 1$ T, we obtain Q ≈ 0.17. However, the stripe model for $Q = 0.17$ and A $= 15$ pJ/m predicts in-plane magnetization for films thickness below 71 nm, a value larger than that for the films studied here, having values below 60 nm. Decreasing Q will increase the range of film thickness with in-plane magnetization. The same calculation for $Q = 0.15$, that can be obtained by adding the in-plane ME anisotropy, increases the critical thickness up to 78 nm. Therefore, a simple estimation for the volume perpendicular anisotropy, if it were present in the films, does not explain the domain structure observed as the gallium content increases.

3.1.2. Surface anisotropy on the Fe-MgO interface and canting

Several works indicate that the anisotropy constant, K_s, due to Fe/non-metallic interfaces can be large. This is because of the perpendicular magnetic orientation observed in thin Fe layers sandwiched by MgO blocks [30] and the canting of M in Fe/MgO films [31]. K_s can be as large as 2 mJ/m^2 and first principles calculations give values of about 3 mJ/m^2 for an ideal MgO/Fe interface [10].

Micromagnetic models [32, 33] analyze the canting of the magnetization due to a surface/interface contribution assuming that the tilting angle can change only along the axial direction and is uniform on each film plane. Both models do not consider the presence of a domain structure, but the results of those analyses provide a starting point to analyze the effect of K_s. Thus, the magnetization state can be in a canted phase, in certain range of film thicknesses, between perpendicular and in-plane magnetization state [33]. In order to find the critical thickness for which FeGa/MgO is in the canted state we use $\mu_0 M_s = 1.2$ T and A$= 15$ pJ/m. In ref. [33] a phase diagram is presented for symmetric structures,

12

but expressions for asymmetrical interface anisotropies are also obtained. For the Fe/Mo interface K_s is probably positive and large because a value of about 2 mJ/m^2 is reported for Mo/CoFeB layers [34]. Therefore, a first analysis is done with the same value of K_s for both interfaces, having in mind that lower values of K_s would reinforce in-plane magnetization. For $K_s = 1.5$ mJ/m^2, the model yields a canted state for films with thickness between 4.6 and 5.5 nm, values well bellow the film thickness. Therefore, although K_s can be large, it is insufficient to deviate **M** from lying on the film plane.

3.2. Random and coherent magnetic anisotropy: thin film vs bulk

Several models, calculations and experiments deal with the effects that the presence of a random magnetic anisotropy (RMA), added to the coherent magnetic anisotropy term, has on the magnetic behavior of crystalline materials[35, 36, 37]. A ferromagnetic with wandering axis (FWA) phase, a magnetic state with the magnetization twisting around the magnetic easy axis, is proposed as the result of the competition between coherent and weak random contributions. Therefore the magnetic order is ferromagnetic but the random anisotropies induce local axis and a deviation of the magnetization vector inside the ferromagnetic domain [35]. $Dy_{100-x}Y_xAl_2$ is a system with weak random anisotropy, generated by dilution of the Y non-magnetic ion, and with coherent cubic anisotropy showing in its phase diagram the presence of a ferromagnetic phase with low remanence between the ferromagnetic and the spin glass phases [36]. Montecarlo simulations also predict a domain ferromagnetic phase, in between of the ordinary ferromagnetic and spin-glass phases in a cubic spin model with random anisotropic exchange for three component spins [37].

A consequence of the presence of RMA in magnets with a coherent anisotropy is that the saturation magnetization approach law in a FWA state is given by the expression [35]:

$$\frac{M(H) - M_s}{M_s} = \frac{1}{15} \frac{H_r^2}{[H_{ex}^3(H + H_c)]^{1/2}} \tag{1}$$

where H_{ex}, H_r and H_c correspond to the exchange, random and coherent

anisotropy fields defined in ref [35]. Considering $\mu_0 H_c M_s = (1/4)K_1$, we obtain $H_c = 2 \times 10^3 A/m$ for $M_s = 10^6 \mathrm{A/m}$ and $|K_1| = 10 \mathrm{\ kJ/m^3}$. The high field magnetization curve measured in film 28-56 is simulated (see red curve Fig 2) with $H_c \approx 2 \times 10^3 A/m$ and $H_r^2/H_{ex}^{3/2} = 1.5 \times 10^4 \sqrt{A/m}$. Therefore, the presence of FWA state can explain the experimental magnetization process.

Another output of this model is that the magnetic correlation length is given by $\delta_m = [A_r/K]^{1/2}$ [35]. With values for $A_r = 15 \mathrm{\ pJ/m}$ and $K = K_1$, $\delta_m \approx 40$ nm. This value is clearly smaller that the corrugation observed by MFM. However the MFM images show the whole landscape of the magnetic state, therefore the transitions between regions with different orientation of M cannot be performed by sharp domain walls, because the exchange energetic cost, and, at least, would require several units of segments with length δ_m. Thus, the oscillation of the magnetic signal is the result of the twist of M in several steps, each one with a length of about δ_m. We note that the periodicity of the domain structure in RMA films with values larger than δ_m has been observed previously in TbFe$_2$ amorphous films [38].

The effect of the disorder due to defects depends on the strength of the local magnetic anisotropy compared with other microscopic parameters. Usually local disorder is small and unable to break the long range correlation length, thus microscopic images show homogeneous areas separated by domain walls, although polycrystalline films can show a ripple of the **M** [15]. Defects existing in FeGa samples with low Ga content and different preparation procedures show uniform magnetization in the single domain areas separated by domain walls. The defects manifest themselves via the domain walls pinning and, hence, modifying the coercive field.

Here, the differences between bulk samples and thin films are presented to explain the presence of random anisotropies in the films that justify the breaking of a uniform orientation of **M** in each magnetic domain. The variation of NNN Ga-Ga distribution in the film, the microstrain in grains and the interface magnetic anisotropy are discussed. All the above factors increase the RMA contributions to the energy with the Ga content.

14

3.2.1. Ga-Ga pairing mechanism

NNN Ga-Ga pairs are able to generate a local strain and therefore a large magnetic anisotropy. The model to explain the variation of the cubic coherent anisotropy [6] suggests that the anisotropy constant of each pair can be large, $\sim 10^7$ J/m^3, but spatial averaging results in an effective fourfold anisotropy about 2-3 orders of magnitude smaller. In thin films, an anisotropic distribution of Ga-Ga pairs between the in-plane and the out-of plane direction is proposed to produce a contribution to the perpendicular anisotropy as large as $\sim 10^5$ J/m^3 [7]. However, the distribution of the Ga-Ga pairs can be inhomogeneous due to the nucleation of ordered FeGa phases. Local fluctuations of the Ga-Ga pairs distribution break the translation symmetry assumed in refs [6, 7] to obtain the macroscopic values of the anisotropy coefficients.

Let us assume that the local anisotropy is generated by the Ga-Ga pairs. In an A2 matrix the distribution of Ga-Ga pairs is homogeneous on the whole volume of the film, independently of the grain size, and each grain has a similar contribution to the anisotropy energy, as happens in a single element film. Increasing the Ga content introduces a metastable state with an ordered secondary phase, and the distribution of those Ga-Ga pairs becomes non-homogeneous since it is random in the volume of the A2 phase and fixed in the inclusions. That number of pairs is null in the D0$_3$ structure, but above the average value of the A2 phase for the B2 structure.

3.2.2. Grain size and micro-strain

Another feature observed in the thin film concerns the comparison of ΔK obtained in this study with bulk samples [39]. $\Delta K_{(002)}$ in the films is at least one order of magnitude smaller for bulk samples, while $\Delta K_{(001)}$ takes values of the same order of magnitude for both kind of samples. In bulk material the volume of the secondary phase is small compared with the main phase and secondary phase zones can behave as pinning centers for domain walls. However, in thin films the analysis of the peak widths suggests that the volume of the grains of each phase is small. On the other hand, the observation of an inhomogeneous

15

strain in the film suggests another mechanism to alter locally the magnetic anisotropy through the ME effect in each grain on the film.

3.2.3. Interface magnetic anisotropy

Last but no least, at the film interface with MgO, the local fluctuations of the Fe/Ga atoms distribution can introduce another source of randomness since the interface contribution per atom is expected to disappear for the Ga-O bond. The ordered phases are formed by two kind of layers, Fe atoms and an ordered mix of Fe and Ga atoms. Thus, the larger value of K_s will be expected for grains that a layer without Ga atoms at the interface has, as happens for one half of the layers of the $D0_3$ and B2 structures; in areas with layers having gallium, K_s will be halved for the $D0_3$ phase or nulled for the B2 one. For the disordered phase the interface contribution will be proportional to the Fe composition and K_s will go with $100\text{-}x/100$.

4. Conclusions

In epitaxial thin films of FeGa grown on MgO(001) substrates, the magnetic domain structure evolves from a uniform in-plane magnetization to a state with a non-collinear configuration as the Ga content increases. The crystalline phase distribution can generate local inhomogeneous distributions of Fe/Ga atoms throughout the film volume and on the interface with the MgO substrate as well as local strains and modify the magnetic anisotropy. Therefore, to explain the observed domain structures, we propose a random magnetic anisotropy associated with such non-homogeneous distributions. This contribution is capable of distorting the magnetization, otherwise uniform within the domains, if only coherent cubic magnetic anisotropy would exist, as happens in bulk samples.

5. Acknowledgments

16

References

[1] A. E. Clark, J. B. Restorff, M. Wun-Fogle, T. A. Lograsso, D. L. Schlagel, Magnetostrictive properties of body-centered cubic Fe-Ga and Fe-Ga-Al alloys, IEEE Trans. Magn. 36 (5 I) (2000) 3238–3240. `doi:10.1109/20.908752`.

[2] A. E. Clark, M. Wun-Fogle, J. Restorff, T. Lograsso, J. Cullen, Effect of quenching on the magnetostriction on Fe_{1-x} Ga_x (0.13< x <0.21), IEEE Trans. Magn. 37 (4) (2001) 2678–2680. `doi:10.1109/20.951272`.

[3] A. E. Clark, K. B. Hathaway, M. Wun-Fogle, J. B. Restorff, T. A. Lograsso, V. M. Keppens, G. Petculescu, R. A. Taylor, Extraordinary magnetoelasticity and lattice softening in bcc Fe-Ga alloys, J. Appl. Phys. 93 (10 3) (2003) 8621–8623. `doi:10.1063/1.1540130`.

[4] H. Yangkun, K. Xiaoqin, J. Chengbao, M. Naihua, W. Hui, C. J. M. David, W. Yunzhi, X. Huibin, Interaction of Trace Rare-Earth Dopants and Nanoheterogeneities Induces Giant Magnetostriction in Fe-Ga Alloys, Adv. Funct. Mater. 28 (20) (2018) 1800858. `doi:10.1002/adfm.201800858`.

[5] O. Ikeda, R. Kainuma, I. Ohnuma, K. Fukamichi, K. Ishida, Phase equilibria and stability of ordered b.c.c. phases in the Fe-rich portion of the Fe–Ga system, J. Alloys Compd. 347 (1) (2002) 198 – 205. `doi:10.1016/S0925-8388(02)00791-0`.

17

URL http://www.sciencedirect.com/science/article/pii/S0925838802007910

[6] J. Cullen, P. Zhao, M. Wuttig, Anisotropy of crystalline ferromagnets with defects, J. Appl. Phys. 101 (12) (2007) 123922. doi:10.1063/1.2749471.
URL https://doi.org/10.1063/1.2749471

[7] M. Barturen, J. Milano, M. Vásquez-Mansilla, C. Helman, M. A. Barral, A. M. Llois, M. Eddrief, M. Marangolo, Large perpendicular magnetic anisotropy in magnetostrictive $Fe_{1-x}Ga_x$ thin films, Phys. Rev. B 92 (2015) 054418. doi:10.1103/PhysRevB.92.054418.
URL http://link.aps.org/doi/10.1103/PhysRevB.92.054418

[8] S. Tacchi, S. Fin, G. Carlotti, G. Gubbiotti, M. Madami, M. Barturen, M. Marangolo, M. Eddrief, D. Bisero, A. Rettori, M. G. Pini, Rotatable magnetic anisotropy in a $Fe_{0.8}Ga_{0.2}$ thin film with stripe domains: Dynamics versus statics, Phys. Rev. B 89 (2014) 024411. doi:10.1103/PhysRevB.89.024411.
URL http://link.aps.org/doi/10.1103/PhysRevB.89.024411

[9] B. Dieny, M. Chshiev, Perpendicular magnetic anisotropy at transition metal/oxide interfaces and applications, Rev. Mod. Phys. 89 (2017) 025008. doi:10.1103/RevModPhys.89.025008.
URL https://link.aps.org/doi/10.1103/RevModPhys.89.025008

[10] H. X. Yang, M. Chshiev, B. Dieny, J. H. Lee, A. Manchon, K. H. Shin, First-principles investigation of the very large perpendicular magnetic anisotropy at Fe|MgO and Co|MgO interfaces, Phys. Rev. B 84 (2011) 054401. doi:10.1103/PhysRevB.84.054401.
URL https://link.aps.org/doi/10.1103/PhysRevB.84.054401

[11] S. Manipatruni, D. E. Nikonov, C.-C. Lin, T. A. Gosavi, H. Liu, B. Prasad, Y.-L. Huang, E. Bonturim, R. Ramesh, I. A. Young, Scalable energy-efficient magnetoelectric spin-orbit logic, Nature 565 (2019) 35. doi:

18

425   10.1038/s41586-018-0770-2.

URL https://doi.org/10.1038/s41586-018-0770-2

[12] T. Maruyama, Y. Shiota, T. Nozaki, K. Ohta, N. Toda, M. Mizuguchi, A. A. Tulapurkar, T. Shinjo, M. Shiraishi, S. Mizukami, Y. Ando, Y. Suzuki, Large voltage-induced magnetic anisotropy change in a few atomic layers

430   of iron, Nat. Nanotechnol. 4 (2009) 158. doi:10.1038/nnano.2008.406.

URL https://doi.org/10.1038/nnano.2008.406

[13] M. A. Marioni, N. Pilet, T. V. Ashworth, R. C. O'Handley, H. J. Hug, Remanence due to Wall Magnetization and Counterintuitive Magnetometry Data in 200-nm Films of Ni, Phys. Rev. Lett. 97 (2006) 027201. doi:

435   10.1103/PhysRevLett.97.027201.

URL http://link.aps.org/doi/10.1103/PhysRevLett.97.027201

[14] R. Frömter, H. Stillrich, C. Menk, H. P. Oepen, Imaging the cone state of the spin reorientation transition, Phys. Rev. Lett. 100 (2008) 207202. doi:10.1103/PhysRevLett.100.207202.

440   URL http://link.aps.org/doi/10.1103/PhysRevLett.100.207202

[15] H. W. Fuller, M. E. Hale, Determination of magnetization distribution in thin films using electron microscopy, J. Appl. Phys. 31 (2) (1960) 238–248. doi:10.1063/1.1735552.
URL https://doi.org/10.1063/1.1735552

445 [16] K. J. Harte, Theory of large-angle ripple in magnetic films, Journal of Applied Physics 37 (3) (1966) 1295–1296. doi:10.1063/1.1708441.
URL https://doi.org/10.1063/1.1708441

[17] M. Ciria, M. G. Proietti, E. C. Corredor, D. Coffey, A. Begué, C. de la Fuente, J. I. Arnaudas, A. Ibarra, Crystal structure and local ordering

450   in epitaxial $Fe_{100-x}Ga_x$/MgO(001) films, J. Alloys Compd. 767 (2018) 905–914. doi:10.1016/j.jallcom.2018.07.120.
URL   https://www.scopus.com/inward/record.uri?eid=2-s2.

0-85050115007&doi=10.1016%2fj.jallcom.2018.07.120&partnerID=
40&md5=5a54548bc22499719746bd58bcea51d9

[18] C. Boubeta-Martínez, J. L. Costa-Krämer, A. Cebollada, Epitaxy, magnetic and tunnel properties of transition metal/MgO(001) heterostructures, J Phys: Condens Matter 15 (25) (2003) R1123–R1167. doi:10.1088/0953-8984/15/25/202.

[19] C. Mudivarthi, S. M. Na, R. Schaefer, M. Laver, M. Wuttig, A. B. Flatau, Magnetic domain observations in Fe-Ga alloys, J. Magn. Magn. Mater. 322 (14) (2010) 2023–2026. doi:10.1016/j.jmmm.2010.01.027.
URL http://dx.doi.org/10.1016/j.jmmm.2010.01.027

[20] Q. Xing, T. A. Lograsso, Magnetic domains in magnetostrictive Fe–Ga alloys, Appl. Phys. Lett. 93 (18) (2008) 182501. doi:10.1063/1.3013575.
URL https://doi.org/10.1063/1.3013575

[21] Y. He, J. M. D. Coey, R. Schaefer, C. Jiang, Determination of bulk domain structure and magnetization processes in bcc ferromagnetic alloys: Analysis of magnetostriction in $Fe_{83}Ga_{17}$, Phys. Rev. Materials 2 (2018) 014412. doi:10.1103/PhysRevMaterials.2.014412.
URL https://link.aps.org/doi/10.1103/PhysRevMaterials.2.014412

[22] S. Rafique, J. R. Cullen, M. Wuttig, J. Cui, Magnetic anisotropy of FeGa alloys, J. Appl. Phys. 95 (11 II) (2004) 6939–6941. doi:10.1063/1.1676054.

[23] A. McClure, S. Albert, T. Jaeger, H. Li, P. Rugheimer, J. A. Schaefer, Y. U. Idzerda, Properties of single crystal $Fe_{1-x}Ga_x$ thin films, J. Appl. Phys. 105 (7) (2009) 07A938. doi:10.1063/1.3077207.
URL http://link.aip.org/link/JAPIAU/v105/i7/p07A938/s1&Agg=doi

[24] G. Williamson, W. Hall, X-ray line broadening from filed aluminium and wolfram, Acta Metall. 1 (1) (1953) 22 – 31.

doi:10.1016/0001-6160(53)90006-6.

URL http://www.sciencedirect.com/science/article/pii/
0001616053900066

[25] T. D. Shen, R. B. Schwarz, J. D. Thompson, Soft magnetism in mechan-
ically alloyed nanocrystalline materials, Phys. Rev. B 72 (2005) 014431.
doi:10.1103/PhysRevB.72.014431.
URL https://link.aps.org/doi/10.1103/PhysRevB.72.014431

[26] N. Kawamiya, K. Adachi, Y. Nakamura, Magnetic Properties and
Mössabauer Investigations of Fe-Ga Alloys, J. Phys. Soc. Jpn. 33 (5) (1972)
1318–1327. doi:10.1143/JPSJ.33.1318.
URL https://doi.org/10.1143/JPSJ.33.1318

[27] A. Hubert, R. Schäfer, Magnetic Domains, Springer-Verlag Berlin Heidel-
berg, 1998.

[28] C. Bormio-Nunes, M. a. Tirelli, R. S. Turtelli, R. Groössinger, H. Muöller,
G. Wiesinger, H. Sassik, M. Reissner, Volume magnetostriction and struc-
ture of copper mold-cast polycrystalline Fe-Ga alloys, J. Appl. Phys. 97 (3)
(2005) 033901. doi:10.1063/1.1834692.

[29] J. Atulasimha, A. B. Flatau, J. R. Cullen, Analysis of the effect of gallium
content on the magnetomechanical behaviour of single-crystal FeGa alloys
using an energy-based method, Smart Mater. Struct. 17 (2008) 025027.
doi:10.1088/0964-1726/20/4/043001.

[30] J. Balogh, I. Dézsi, C. Fetzer, J. Korecki, A. Kozioł-Rachwał, E. Młyńczak,
A. Nakanishi, Magnetic properties of the Fe-MgO interface studied by
Mössbauer spectroscopy, Phys. Rev. B 87 (2013) 174415. doi:10.1103/
PhysRevB.87.174415.
URL https://link.aps.org/doi/10.1103/PhysRevB.87.174415

[31] T. Kawauchi, Y. Miura, X. Zhang, K. Fukutani, Interface-driven non-
collinear magnetic structure and phase transition of Fe thin films, Phys.

21

Rev. B 95 (2017) 014432. `doi:10.1103/PhysRevB.95.014432`.

510   URL `https://link.aps.org/doi/10.1103/PhysRevB.95.014432`

[32] R. C. O'Handley, J. P. Woods, Static magnetization direction under perpendicular surface anisotropy, Phys. Rev. B 42 (1990) 6568–6573. `doi:10.1103/PhysRevB.42.6568`.
URL `https://link.aps.org/doi/10.1103/PhysRevB.42.6568`

515 [33] A. Thiaville, A. Fert, Twisted spin configuration in thin magnetic layers with interface anisotropy, J. Magn. Magn. Mater. 113 (1992) 161. `doi:10.1016/0304-8853(92)91263-S`.

[34] T. Liu, Y. Zhang, J. W. Cai, H. Y. Pan, Thermally robust Mo/CoFeB/MgO trilayers with strong perpendicular magnetic anisotropy, Sci. Rep. 4 (2014) 520   5895. `doi:10.1038/srep05895`.
URL `https://doi.org/10.1038/srep05895`

[35] E. M. Chudnovsky, W. M. Saslow, R. A. Serota, Ordering in ferromagnets with random anisotropy, Phys. Rev. B 33 (1986) 251–261. `doi:10.1103/PhysRevB.33.251`.

525   URL `https://link.aps.org/doi/10.1103/PhysRevB.33.251`

[36] A. del Moral, J. I. Arnaudas, P. M. Gehring, M. B. Salamon, C. Ritter, E. Joven, J. Cullen, Magnetic first-order phase transition and crossover associated with random anisotropy in crystalline $Dy_xY_{1-x}Al_2$, Phys. Rev. B 47 (1993) 7892–7896. `doi:10.1103/PhysRevB.47.7892`.

530   URL `https://link.aps.org/doi/10.1103/PhysRevB.47.7892`

[37] R. Fisch, Phase transitions in cubic models with random anisotropic exchange, Phys. Rev. B 51 (1995) 6358–6363. `doi:10.1103/PhysRevB.51.6358`.
URL `https://link.aps.org/doi/10.1103/PhysRevB.51.6358`

535 [38] F. Hellman, A. L. Shapiro, E. N. Abarra, R. A. Robinson, R. P. Hjelm, P. A. Seeger, J. J. Rhyne, J. I. Suzuki, Long ferromagnetic correlation

length in amorphous $TbFe_2$, Phys. Rev. B 59 (1999) 11408–11417. `doi:10.1103/PhysRevB.59.11408`.

URL `https://link.aps.org/doi/10.1103/PhysRevB.59.11408`

[39] Y. Du, M. Huang, T. a. Lograsso, R. J. McQueeney, X-ray diffuse scattering measurements of chemical short-range order and lattice strains in a highly magnetostrictive $Fe_{0.813}Ga_{0.187}$ alloy in an applied magnetic field, Phys. Rev. B 85 (21) (2012) 214437. `doi:10.1103/PhysRevB.85.214437`.